

Electronic structure near the 1/8-anomaly in La-based cuprates

J. Chang¹, Y. Sassa¹, S. Guerrero², M. Månsson^{1,3}, M. Shi⁴, S. Pailh s¹, A. Bendounan¹, R. Mottl¹, T. Claesson³, O. Tjernberg³, L. Patthey⁴, M. Ido⁵, M. Oda⁵, N. Momono^{5,6}, C. Mudry² and J. Mesot^{1,7}

¹ Laboratory for Neutron Scattering, ETH Zurich and PSI Villigen, CH-5232 Villigen PSI, Switzerland

² Condensed Matter Theory Group, Paul Scherrer Institute, CH-5232 Villigen PSI, Switzerland

³ Materials Physics, Royal Institute of Technology KTH, S-164 40 Kista, Sweden

⁴ Swiss Light Source, Paul Scherrer Institute, CH-5232 Villigen PSI, Switzerland

⁵ Department of Physics, Hokkaido University - Sapporo 060-0810, Japan

⁶ Department of Materials Science and Engineering, Muroran Institute of Technology, Muroran 050-8585, Japan

⁷ Institut de la mati re complexe, Ecole Polytechnique F d d rale de Lausanne (EPFL), CH-1015 Lausanne, Switzerland

Abstract. We report an angle resolved photoemission study of the electronic structure of the pseudogap state in $\text{La}_{1.48}\text{Nd}_{0.4}\text{Sr}_{0.12}\text{CuO}_4$ ($T_c < 7$ K). Two opposite dispersing Fermi arcs are the main result of this study. The several scenarios that can explain this observation are discussed.

Submitted to: *New J. Phys.*

1. Introduction

Deciphering the microscopic mechanism responsible for high-temperature (high- T_c) superconductivity has remained an elusive challenge for 20 years. Progress has been held back by the difficulty to characterize and understand the all but conventional normal states from which high- T_c superconductivity emerges in the underdoped and optimally doped regimes, respectively. For example, the pseudogap state – the normal state of underdoped high- T_c superconductors – is characterized by two properties that are difficult to reconcile. First, angular resolved photoemission spectroscopy (ARPES) studies of the electronic structure in the pseudogap state have revealed the existence of hole-like arcs centered around the diagonal of the Brillouin zone supporting gapless quasiparticles [1, 2, 3, 4]. Fermi arcs cannot be attributed to a Fermi liquid (FL): the Fermi surface of a FL can only terminate at the boundary of the Brillouin zone. Second, transport measurements in high-magnetic field have revealed the existence of quantum oscillations in the pseudogap state of $\text{YBa}_2\text{CuO}_{7+\delta}$ [5, 6, 7, 8] (YBCO). Quantum oscillations come about when quasiparticles are orbiting around a closed Fermi surface. These and other hallmarks of the pseudogap state has lead to two conflicting interpretations; either the pseudogap state is a precursor to superconductivity or it is related to an order that competes with superconductivity [9, 10, 11].

Here we show by ARPES that the electronic structure in the pseudogap state of $\text{La}_{1.48}\text{Nd}_{0.4}\text{Sr}_{0.12}\text{CuO}_4$ ($T_c < 7\text{K}$) consists of two oppositely dispersing arcs. We present furthermore a systematic study of the normal state electronic structure of Nd-free $\text{La}_{2-x}\text{Sr}_x\text{CuO}_4$ near the 1/8-anomaly. The possible origins of the second arc is discussed and we show that it can be naively modeled by assuming the existence of a Fermi pocket.

2. Methods

Our $\text{La}_{1.48}\text{Nd}_{0.4}\text{Sr}_{0.12}\text{CuO}_4$ sample, grown by the traveling-solvent floating-zone method, has $T_c < 7$ K. Previous μSR and neutron diffraction experiments on the same sample are published in Refs. [12] and [13]. The ARPES experiments were performed at the SIS-beamline of the Swiss Light Source (SLS) at the Paul Scherrer Institute (PSI) using 55 eV circular polarized light. The overall momentum resolution was 0.15 degrees and the pseudogap was measured with an energy resolution of ~ 18 meV. The measurements were preformed under ultra-high vacuum condition and the samples were cleaved at the temperature $T = 15$ K. (The lowest accessible temperature on this instrument, $T \approx 10$ K, remains above T_c .) The ARPES data presented here were recorded in the second Brillouin zone but presented in the first zone for convenience. The Fermi level was determined from a spectrum recorded on polycrystalline copper on the sample holder.

3. Results

3.1. Nodal and anti-nodal spectrum

Figures 1(a) and 1(b) show two typical ARPES spectra collected close to the M-Y (zone boundary/anti-nodal) and Γ -Y (zone diagonal/nodal) directions (see inset) in an incommensurate antiferromagnetic and charge ordered phase (the so-called stripe phase) of $\text{La}_{1.48}\text{Nd}_{0.4}\text{Sr}_{0.12}\text{CuO}_4$ (NdLSCO) at $T = 15$ K, *i.e.*, well above the superconducting T_c . The ARPES intensity is displayed in a false color scale as a function of binding energy ω and momentum \mathbf{k} as indicated in the inset. The spectra can be analyzed with the help of constant-momentum cuts called energy distribution curves (EDC) or constant-energy cuts called momentum distribution curves (MDC). The white points in Figs. 1(a) and 1(b) define MDC at the Fermi level E_F that can be fitted by (double) Lorentzian's with a linear background. In doing so, the characteristic momenta \mathbf{k}_F depicted by circles and stars in Fig. 2 can be identified. This set of \mathbf{k}_F defines the *underlying Fermi surface* shown in Fig. 2.

In Fig. 1(c) we contrast the EDC at $\mathbf{k} = \mathbf{k}_F^a$ and $\mathbf{k} = \mathbf{k}_F^b$, *i.e.*, for parts of the underlying Fermi surface close to the boundary and diagonal of the Brillouin zone, respectively. An intense spectral peak with the leading edge reaching E_F is observed along cut (b) whereas no spectral peak is visible in the spectrum of cut (a). Moreover, the leading edge along cut (a) is shifted away from E_F , thereby revealing the existence of a gap Δ consistent with the pseudogap observed in the normal state of underdoped cuprates. We used the so-called symmetrization method to factor out the Fermi distribution [1]. As in strongly underdoped $\text{Bi}_2\text{Sr}_2\text{CaCuO}_2$ (Bi2212) [14], our symmetrized EDC exhibit inflection points that can be used to extract the momentum dependence of the pseudogap Δ . It is shown in Fig. 1(d) that $\Delta(\pi, 0) \approx 30 \pm 5$ meV which is comparable with a recent ARPES report on $\text{La}_{2-x}\text{Ba}_x\text{CuO}_4$ at $x \approx 1/8$ [15]; another compound displaying a stripe phase. Upon moving towards the zone diagonal, Fig. 3(a) shows that the pseudogap remains approximately constant as a function of the underlying Fermi surface angle $0 < \phi < 15^\circ$ defined in Fig. 2. Moving closer to the diagonal direction, the pseudogap vanishes very fast and for $\phi > 30^\circ$ gapless quasiparticles with an enhanced lifetime are observed, in agreement with past studies of the pseudogap state [2, 3].

3.2. Secondary branch

Remarkably, a careful inspection of the spectra along cut (b) reveals the existence of a second weaker branch of the underlying Fermi surface in the form of a secondary peak in the MDC of Fig. 1(b). This second branch is not an artifact of a small minority grain since it has been observed on a handful of freshly cleaved surfaces. It is also not a consequence of chemical disorder introduced by Nd, since a similar secondary peak was observed in Nd-free $\text{La}_{1.88}\text{Sr}_{0.12}\text{CuO}_4$ (see later). Instead, we believe that this branch is intrinsic and that it carries important information about the electronic structure of the

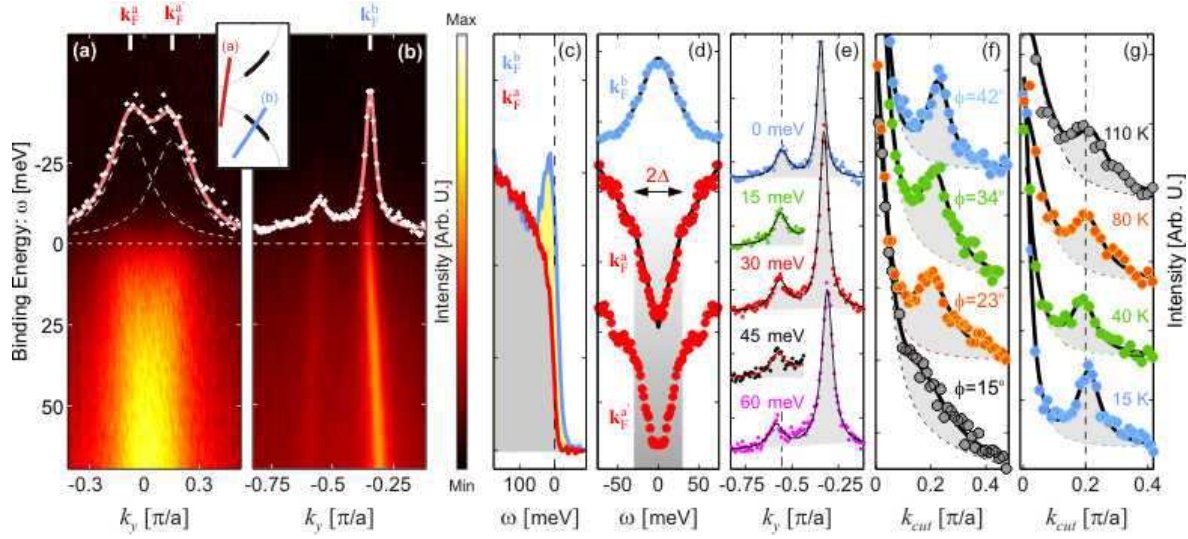


Figure 1. (a)-(b) ARPES intensity measured at $T = 15$ K as a function of binding energy ω and momentum \mathbf{k} along the red and blue cuts shown in the top inset of (b). The ratio of maximum intensity between (a) and (b) is $\sim 3/4$. White points are the momentum distribution curves (MDC) at $\omega = E_F$ and the solid lines are Lorentzian fits with a linear background. The double-peak structure stems from the cuts that are crossing two branches. (c) Energy distribution curves (EDC) at $\mathbf{k} = \mathbf{k}_F^a$ (red) and $\mathbf{k} = \mathbf{k}_F^b$ (blue) for the spectra shown in (a) and (b). (d) Symmetrized EDC for $\mathbf{k} = \mathbf{k}_F^{a,a',b}$. The solid black lines are guides to the eye. (e) MDC at $\omega = 0, 15, 30, 45,$ and 60 meV for the spectra shown in (b). To avoid overlapping of the primary branches, only the secondary branch is displayed when $\omega = 15$ and 45 meV. (f) MDC at $\omega = 3$ meV for four different cuts, showing the secondary branch as a function of the Fermi surface angle ϕ defined in Fig. 2. (g) Temperature dependence of the MDC at $\omega = E_F$ for cut (b). For both (f) and (g) the peak position of each primary branch is centered at zero momentum. The solid lines are Lorentzian fits to a double-peak structure, while the dashed lines show the shape of a single Lorentzian.

pseudogap state.

3.2.1. Momentum dependence of the pseudogap and the MDC-linewidth. Figure 1(e) shows a set of MDC along cut (b) at different energies that reveal the opposite dispersion of the two branches. We find from Fig. 1(e) that the Fermi velocity of the primary ($v_F \approx 1.6 \pm 0.05$ eVÅ) and secondary ($v_F \approx -2.0 \pm 0.3$ eVÅ) branch are consistent with the universal Fermi velocity along the diagonal of hole-doped cuprates [16]. We have followed the evolution of \mathbf{k}_F and the MDC line-width Γ_{MDC} [half width at half maximum (HWHM)] for both branches. The momentum dependence of the secondary branch, relative to that of the primary branch, is shown in Fig. 1(f). The peak separation between the two branches decreases as ϕ decreases from $\phi \approx 45^\circ$ to $\phi \approx 15^\circ$. Figure 3(b) shows the dependence of Γ_{MDC} as a function of ϕ . Along the Fermi arcs we observe, that the line-width is approximately constant $\Gamma_{\text{MDC}} \approx 0.03 \pi/a$ and $\Gamma_{\text{MDC}} \approx 0.05 \pi/a$ for both the primary and secondary branches. However, once the pseudogap opens the

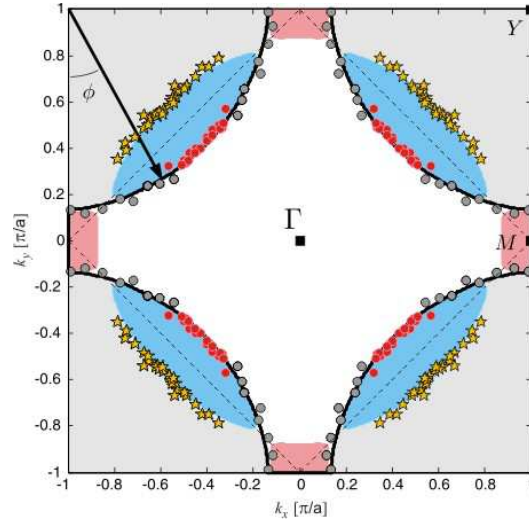


Figure 2. The locations of the peaks in the MDC at E_F define the *underlying Fermi surface* and are denoted by circles and stars. Momenta along the underlying Fermi surface characterized by gapless quasiparticles are denoted by red circles and grey circles denote the part of the Fermi surface where the quasiparticles are suppressed by the pseudogap. The data have been symmetrized with respect to the tetragonal crystal structure. The solid black line stems from the Fermi surface derived from Eq. (4) while the blue and pink colored regions depict the hole and electron pockets predicted from Eq. (6). The dashed lines bound the reduced Brillouin zone.

line-width increases gradually to $\Gamma_{\text{MDC}} \approx 0.13 \pi/a$ for the primary branch at the zone boundary ($\phi = 0^\circ$). Here, $a \approx 3.8 \text{ \AA}$ is the lattice spacing of the CuO square lattice. The simultaneous opening of the pseudogap and the broadening of the MDC line-width make it practically impossible to resolve the secondary branch once it appears as a weak shoulder on the primary branch below $\phi \approx 15^\circ$, *i.e.*, close to $(\pi, 0)$ [see grey circles in Fig. 1(f)].

The underlying Fermi surface defined by the positions of the MDC peaks at E_F is shown in Fig. 2. The circles identify the primary branch, that can be followed all the way to the zone boundary. The red circles map out four primary Fermi arcs by the criterion that gapless quasiparticle peaks [see blue curve in Fig. 1(c)] are observed while the grey points map out the segments of the underlying Fermi surface where the quasiparticle peaks are suppressed by the pseudogap. The gapless quasiparticles have a finite lifetime along the primary Fermi arcs. A more delicate analysis is needed to extract the quasiparticle lifetimes of the secondary branch as it requires a background subtraction in order to observe EDC peaks (see Appendix A). Here, we only display the Fermi momenta of the secondary branch by the stars in Fig 2.

3.2.2. Temperature dependence of the secondary branch and the pseudogap. We now turn to the temperature dependence of the secondary branch along cut (b). No significant change of the intensity of the secondary branch for $\omega = E_F$ is observed for

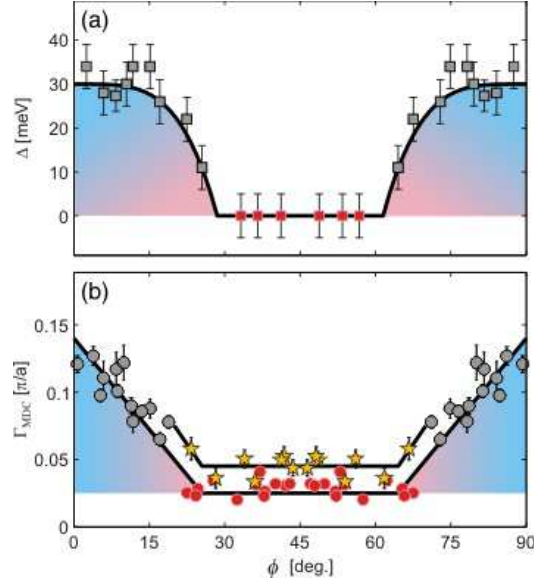


Figure 3. (a) The pseudogap Δ as a function of the polar angle ϕ defined in Fig. 2. (b) Γ_{MDC} as a function of ϕ , circular and star points represent the primary and secondary branches, respectively. The solid lines are guides to the eye.

upon heating from $T = 15$ K to $T = 110$ K (see Fig. 1(f)). Figures 4(a1-a3) show the ARPES spectra recorded along cut (a) of Fig. 1 for $T = 15$, 40, and 80 K while Fig. 4(b1-b3) show the spectra recorded along cut (b) for $T = 40$, 80, and 110 K. The white points in Figs. 4(a1-a3) and Figs. 4(b1-b3) are the momentum distribution curves (MDC) at $\omega = E_F$ while the solid lines are double Lorentzian fits with a linear background. For each MDC, the double Lorentzian fit allows to extract the MDC linewidth $\Gamma_{\text{MDC}}^{(\text{cut})}$. The dependence on the temperature T of the MDC linewidths along cut (a), $\Gamma_{\text{MDC}}^{(a)}$, and along cut (b), $\Gamma_{\text{MDC}}^{(b)}$, is shown in Fig. 4(c) by the red and black circles, respectively. The temperature dependence can, to a first approximation, be described by

$$\Gamma_{\text{MDC}}^{(\text{cut})}(T) = \alpha^{(\text{cut})} + \beta^{(\text{cut})}T. \quad (1)$$

For cut (a) the linewidth is roughly temperature independent, thus

$$\alpha^{(a)} \approx 0.0106 \pi/a, \quad \beta^{(a)} \approx 0, \quad (2)$$

see the horizontal dashed line in Fig. 4(c). By contrast for cut (b) the linewidth exhibits a stronger temperature dependence and a least-square fit yields

$$\alpha^{(b)} = 0.0132 \pi/a, \quad \beta^{(b)} = 0.0006 \pi/(aK), \quad (3)$$

as shown by the solid red line in Fig. 4(c).

The evolution with temperature of the spectra shown in Figs. 4(b1-b3) demonstrates that both the pseudogap and the secondary Fermi arcs persist deep into the low-temperature orthorhombic (LTO) phase. Hence, neither the pseudogap nor the secondary Fermi arcs are directly related to the spin and charge long-range order (LRO) observed by neutron diffraction and μSR experiments, as static stripes appear only in the low-temperature tetragonal (LTT) phase [17, 18, 12].

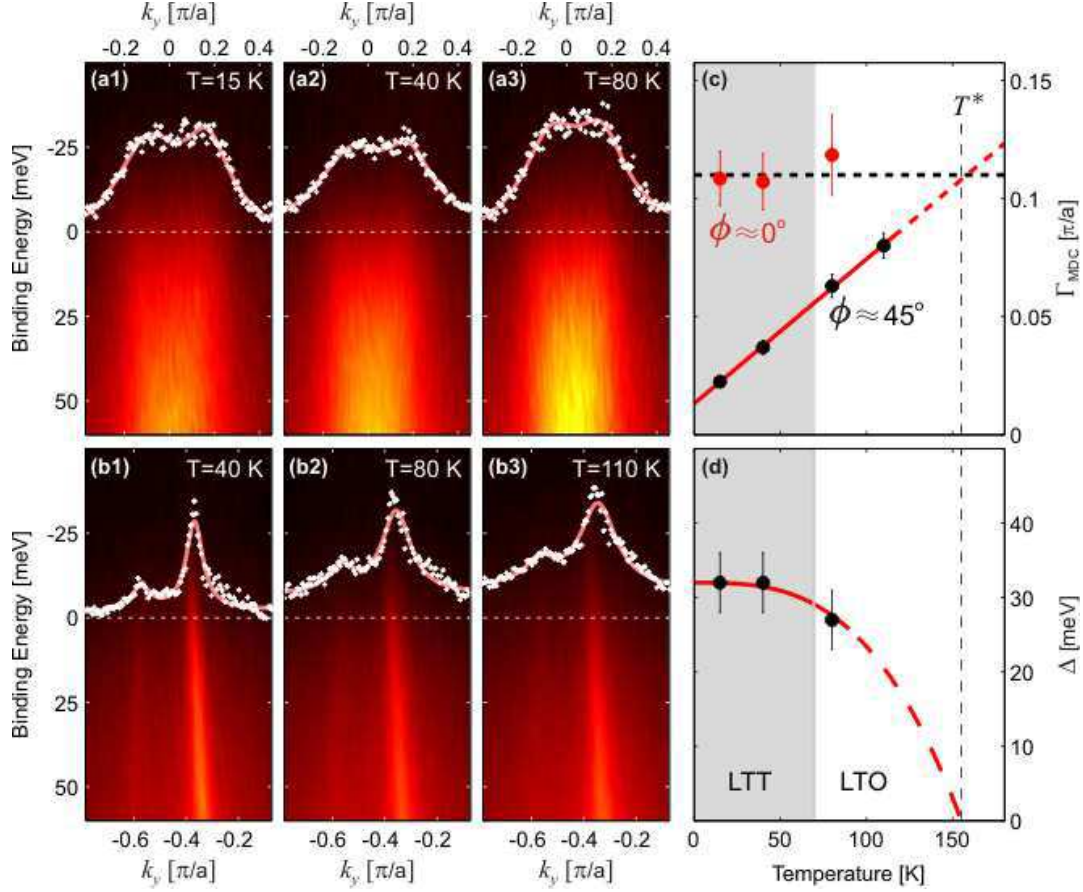


Figure 4. (a1-a3) Cut (a) of the manuscript with $T = 15, 40,$ and 80 K respectively. (b1-b3) are the spectrum along cut (b) of the manuscript with $T = 40, 80,$ and 110 K. White points are momentum distribution curves (MDC) at $\omega = E_F$ and the solid lines are double Lorentzian fits with a linear background. (c) The MDC linewidth at $\omega = E_F$ of cut (a) (red points) and cut (b) (black points) as a function of temperature. The solid red line is a linear fit. (d) The pseudogap Δ as a function of temperature; the red line is a guide to the eye. T^* is defined by the derivation away from the linear temperature dependence of the in-plane resistivity [19].

4. Crystal structure and doping dependence

Now we turn to discuss the possible origin of the secondary band. Very early on the so-called shadow band was observed in Bi2212 [20]. The shadow band is essentially doping and temperature independent [21]. By use of high-quality untwinned crystals and tunable light polarization [22] the shadow band was later shown to originate from the orthorhombic distorted lattice structure. This shadow band is reminiscent of the secondary band that we have observed in $\text{La}_{1.48}\text{Nd}_{0.4}\text{Sr}_{0.12}\text{CuO}_4$ (NdLSCO). Our NdLSCO crystals is not fully untwinned. For this reason it is not possible to follow the experimental procedure of Ref. [22] to demonstrate whether the secondary branch in NdLSCO has its origin from a weak orthorhombic distortion.

Band structure calculations generically predict that weak orthorhombic distortions

of a tetragonal lattice structure lead to a band folding with $\mathbf{Q} = (\pi, \pi)$ in the tetragonal Brillion zone [23]. Accordingly one would expect to observe hole pockets for any weak orthorhombic distortion of a tetragonal lattice structure. Now, $\text{La}_{2-x}\text{Sr}_x\text{CuO}_4$ has an orthorhombic lattice structure [13] at low temperatures for $x < 0.21$. Sofar there was however little experimental evidence for a shadow band in LSCO. Nakayama *et al.* [25] observed a weak indication of a backfolded band in the superconducting state of $\text{La}_{1.85}\text{Sr}_{0.15}\text{CuO}_4$. X.J. Zhou *et al.* [26] on the other hand observed the secondary band for $x = 0.06$ and 0.09 but not for $x = 0.15$. The latter study thus indicates a rather strong doping dependence of the secondary band that does not correlate with an orthorhombic phase of LSCO in an obvious way. We now present a systematic study of the normal state electronic structure in $\text{La}_{2-x}\text{Sr}_x\text{CuO}_4$ near the 1/8-anomaly. In Fig. 5 cuts (a)-(c), close to the zone diagonal, are shown for $\text{La}_{2-x}\text{Sr}_x\text{CuO}_4$ with $x = 0.105$, $x = 0.12$, and $x = 0.145$, respectively. Interestingly, we observe back folding only for $x = 0.12$, as shown in Fig. 5(b), but not for $x = 0.105$ and $x = 0.145$, as shown in Figs. 5(a) and (c). This strongly suggests that the band folding is enhanced near the so-called 1/8-anomaly (compounds with $x \approx 1/8$).

We now turn our attention to NdLSCO. The average crystal structure of NdLSCO is tetragonal for $T < 69$ K. However, locally each CuO_2 -planes has orthorhombic distortions [27]. Such local distortions could lead to a back folding [28]. However, if the back folding is purely of structural origin, one would expect a significant effect when going from the LTO to the LTT lattice structure. We show in Fig. 1(g) that the intensity of secondary branch displays essentially no change upon going through the LTO-LTT transition.

We have shown that the back folding is strongly enhanced near the so-called 1/8-anomaly and it appears independent of the (local and global) crystal structure. We are therefore lead to the preliminary conclusion that the secondary branch can not be attributed solely to orthorhombic distortions of the tetragonal crystal structure.

5. Discussion

The observation of the secondary branch of excitations at the Fermi energy is the main result of this letter. Whether or not the secondary branch is an effect related to the crystal structure, the electronic structure can be modeled by the use of a tight-binding model. We are now going to argue by appealing to a simple two-dimensional [29] fermiology model, that the primary and secondary Fermi arcs are the remnants of two hidden Fermi pockets: a hole pocket centered at the diagonal and an electron pocket centered at the M-point. The black lines in Fig. 2 are the Fermi surface of the tight-binding dispersion

$$\varepsilon_{\mathbf{k}} = \mu - 2t (\cos k_x a + \cos k_y a) - 4t' \cos k_x a \cos k_y a, \quad (4)$$

where the nearest-neighbor amplitude $t = 240$ meV while the chemical potential $\mu/t = 1$ and the next-nearest-neighbor hopping amplitude $t'/t = -0.325$ are fixed by the Fermi

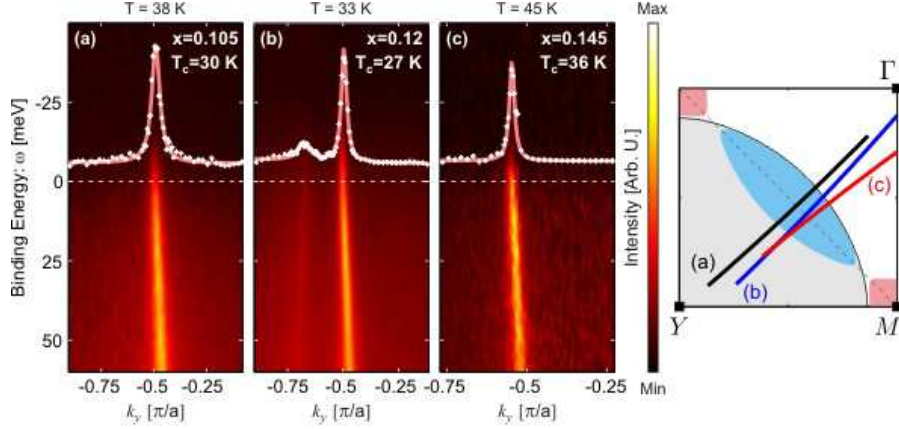


Figure 5. (a)-(c) ARPES intensity as function of binding energy and momentum (shown in right panel) for $\text{La}_{2-x}\text{Sr}_x\text{CuO}_4$ with $x = 0.105$, $x = 0.12$, and $x = 0.145$. The white points in (a)-(c) are momentum distribution curves at $\omega = E_F$ and the solid lines are Lorentzian fits with linear background. (a1)-(c1) show the underlying Fermi surface for $x = 0.105$, $x = 0.12$, and $x = 0.145$. The blue lines indicate the momentum cuts along which the spectra shown in (a)-(a) are recorded.

velocity along the diagonal and topology of the primary branch of the underlying Fermi surface, respectively. The Fermi surface centered around the Y -point has the area

$$A_{FS} = 2(1 + p)A \approx 2.242A \quad (5)$$

where $A = (\pi/a)^2$. Notice that the number $p \approx 0.12$ of charge carriers counted from half filling is consistent with the nominal doping $x = 0.12 \pm 0.005$. Evidently, $\varepsilon_{\mathbf{k}}$ fails to account for the secondary Fermi arc shown in Fig. 2. We observe that \mathbf{k}_F of the primary and secondary branch are approximately related by a reflection symmetry about the reduced zone boundary (see dashed line in Fig. 2). This is suggestive of a unit cell doubling. In a simple fermiology picture, such a unit cell doubling can occur with the onset of long-range order (LRO) in a particle-hole channel at the momentum $\mathbf{Q} = (\pi, \pi)$ that causes the opening of a single-particle gap γ close to the *hot spots* – the crossings between the Fermi surface $\varepsilon_{\mathbf{k}} = 0$ and the reduced zone boundary. This brings about the reconstruction of the Fermi surface $\varepsilon_{\mathbf{k}} = 0$ according to [30]

$$0 = \varepsilon_{\mathbf{k},\mathbf{Q}}^{\pm} \equiv \frac{\varepsilon_{\mathbf{k}} + \varepsilon_{\mathbf{k}+\mathbf{Q}}}{2} \pm \sqrt{\left(\frac{\varepsilon_{\mathbf{k}} - \varepsilon_{\mathbf{k}+\mathbf{Q}}}{2}\right)^2 + \gamma^2}. \quad (6)$$

By choosing the constant single-particle gap $\gamma = 30$ meV the lower branch $\varepsilon_{\mathbf{k},\mathbf{Q}}^{-} \leq 0$ yields the hole pocket shown by the blue area in Fig. 2 [31]. There also exists a small electron pocket ($\varepsilon_{\mathbf{k},\mathbf{Q}}^{+} \leq 0$) centered around $(\pi, 0)$ as indicated by the pink shaded area in Fig. 2. Although we do not provide any direct signature of an electron pocket, our ARPES data are not inconsistent with an electron pocket. It is difficult to extract such information from the spectrum close to the zone boundary because (i) the intensity is strongly suppressed at E_F due to the pseudogap and (ii) Γ_{MDC} is comparable to the diameter of the predicted electron pocket. However, transport measurements on this

material [32, 33] and other so-called stripe compounds [34] have revealed the existence of a negative Hall coefficient at low temperatures; the usual fingerprint of an electron pocket. Assuming that the Luttinger sum rule [36] holds, it can be shown by simple geometrical considerations that p in Eq. 5 becomes

$$p = (A_{hp} - 0.5A_{ep}) / A \approx 0.12 \quad (7)$$

where $A_{hp} = 0.155A = 10.6 \text{ nm}^{-2}$ is the area of the hole pocket and $A_{ep} = 0.064A = 4.4 \text{ nm}^{-2}$ is the volume of the electron pocket in Fig. 2 [37]. The naive two-band structure, suggested in Eq. 6, is one way to reconcile Hall-coefficient and ARPES experiments. So far there exist, however, little spectroscopy evidence for a two-band structure in hole doped cuprates. For electron doped cuprates there exist on the other hand several reports claiming the observation of a two-band structure for dopings slightly larger than $x \sim 1/8$ [38, 39].

The qualitative observation of a hole pocket is compatible with many theories. Band structure calculations have shown that pockets can form in orthorhombic crystal structures [23]. However, the fact that the secondary band is enhanced for $x \approx 0.12$ in orthorhombic $\text{La}_{2-x}\text{Sr}_x\text{CuO}_4$ would suggest that orthorhombic lattice distortions can not be the primary cause for the Fermi surface reconstruction that we observe. Models that invoke spin and charge separation of the electron quantum numbers [10, 40, 41, 42] or competing orders [43, 30, 44, 45, 46] also predict a hole pocket in the pseudogap phase. Moreover, an electron pocket is predicted to coexist with a hole pocket as a result of competing orders [43, 30, 44, 45]. A clue favoring the scenario by which competing order is causing the Fermi-surface reconstruction seen by ARPES in NdLSCO and $\text{La}_{1.88}\text{Sr}_{0.12}\text{CuO}_4$ is the observation of a spin-density wave LRO in these materials [13]. However, the fact that the Fermi surface reconstruction is present above the onset temperature of the spin-density wave LRO suggests that this true LRO is not required for the formation of pockets [43, 30].

6. Conclusions

In summary, our unambiguous observation of a secondary branch of gapless quasiparticles around the zone diagonal in the stripe-compound NdLSCO is consistent with a hole-like Fermi surface induced by a unit cell doubling with the characteristic momentum $\mathbf{Q} = (\pi, \pi)$. Such a secondary branch was also observed in underdoped LSCO ($0.03 < x < 0.06$) by X.J. Zhou *et al.* [26]. Our results on Nd-free LSCO suggest that this secondary branch is enhanced near the so-called 1/8-anomaly. While the results around the 1/8-anomaly might suggest a connection to a spin density wave effect, the non-monotonic doping dependence implies a non-trivial interplay of spin and lattice degrees of freedom.

Acknowledgments

This work was supported by the Swiss NSF (through NCCR, MaNEP, and grant Nr 200020-105151, PBEZP2-122855), the Ministry of Education and Science of Japan and the Swedish Research Council. This work was entirely performed at the Swiss Light Source of the Paul Scherrer Institute, Villigen PSI, Switzerland. We thank the beamline staff of X09LA for their support and we thank M. R. Norman, T. M. Rice, and F. C. Zhang for discussions.

Appendix A. Quasiparticles on the secondary branch

It was shown in the manuscript that gapless spectral peaks are visible along the primary Fermi arc centered around the zone diagonal. We are now going to examine more closely the spectral peaks in the energy distribution curves (EDC) associated to the secondary Fermi arc. Figure A1(a) shows the spectrum along cut (b) at $T = 15$ K. Figure A1(b) shows the EDC at \mathbf{k}_F [determined by the MDC at $\omega = E_F$ and indicated by the blue and red lines in A1(a)] for both the primary and secondary Fermi arcs with blue and red points, respectively. The yellow points sample an EDC with \mathbf{k} chosen sufficiently far from the detector edge but still not too close to the Fermi arcs so as not to cross either the primary or the secondary dispersing branches seen in (a). This EDC may therefore represent an average background intensity observed by ARPES. To better visualize the EDC at \mathbf{k}_F for the secondary Fermi arc, we subtract in Fig. A1(c) the yellow data points from the red data points in Fig. A1(b). Although a peak remains, it is difficult to analyze it so as to extract a quasiparticle lifetime. We thus limit our conclusions to the fact that we observe a weak but significant spectral peak at \mathbf{k}_F on the secondary branch.

Finally we comment on the fate of the secondary branch in the superconducting state of NdLSCO. Since the onset temperature of superconductivity in our NdLSCO sample ($T_c \sim 7$ K) is below the lowest accessible temperature of the SIS instrument, we have not been able to study the secondary branch of NdLSCO in the superconducting state. The effect on the secondary branch upon cooling into the superconducting state of NdLSCO remains therefore an outstanding open problem. However, we were able to confirm that the secondary branch persists into the superconducting state of $\text{La}_{1.88}\text{Sr}_{0.12}\text{CuO}_4$ although the applied energy resolution did not permit the determination of a superconducting gap on the secondary branch.

Appendix B. Temperature dependence of the secondary branch

What could be the energy (temperature) scale that controls the existence of the secondary Fermi arcs? We have argued in the manuscript on the basis of a simple fermiology model that the pseudogap energy scale might be related to the existence of a hole-like Fermi pocket. If so, we would expect that the secondary Fermi arc should

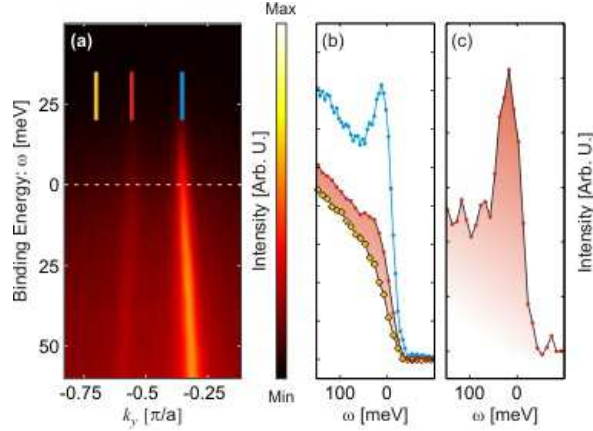


Figure A1. (a) The same ARPES spectrum as shown in Fig. 1(b) of the manuscript. (b) The blue and red points are the energy distribution curves at \mathbf{k}_F located at the primary and secondary Fermi arcs, respectively. The yellow points are a typical energy distribution curve that never crosses the primary and secondary dispersing branches seen in (a). (c) Difference between the red and yellow points in (b).

disappear with increasing temperature at the temperature $T^* \approx 155$ K, below which the pseudogap manifests itself (as measured from the deviation away from the linear temperature dependence of the in-plane resistivity [19]). This expectation is consistent with the observation that the linear fits along cuts (a) and (b) in Eq. (1) intersect at the temperature $T^* \approx 155$ K as shown in Fig. 4(c). Unfortunately, the direct experimental verification of this educated guess is ambiguous due to the thermal broadening of the MDC along cut (b). This is illustrated in Fig. B1 where we plot the double Lorentzian fits to the MDC along (b) at the Fermi energy with their temperature-dependent widths taken from Fig. 4(c), assuming a temperature independent peak amplitude. Whereas it is still possible to extract \mathbf{k}_F and the linewidth of the secondary branch at $T \approx 110$ K this task becomes ambiguous at $T \approx T^* \approx 155$ K as the secondary Fermi arc is signaled by a small shoulder on the dominant peak induced by the primary Fermi arc (see Fig. B1).

References

- [1] Norman, M. R. *et al.* Destruction of the Fermi surface in underdoped high- T_c superconductors. *Nature* **392**, 157-160 (1998).
- [2] Shen, K. M. *et al.* Nodal Quasiparticles and Antinodal Charge Ordering in $\text{Ca}_{2-x}\text{Na}_x\text{CuO}_2\text{Cl}_2$. *Science* **307**, 901-904 (2005).
- [3] Kanigel, A. *et al.* Evolution of the pseudogap from Fermi arcs to the nodal liquid. *Nature Physics* **2**, 447-451 (2006).
- [4] Hossain M. A. *et al.* Controlling the self-doping of $\text{YBa}_2\text{Cu}_3\text{O}_{7-\delta}$ polar surfaces: From Fermi surface to nodal Fermi arcs by ARPES. *Nature Physics* **4**, 527 (2008)
- [5] Doiron-Leyraud, N. *et al.* Quantum oscillations and the Fermi surface in an underdoped high- T_c superconductor. *Nature* **447**, 565-568 (2007).

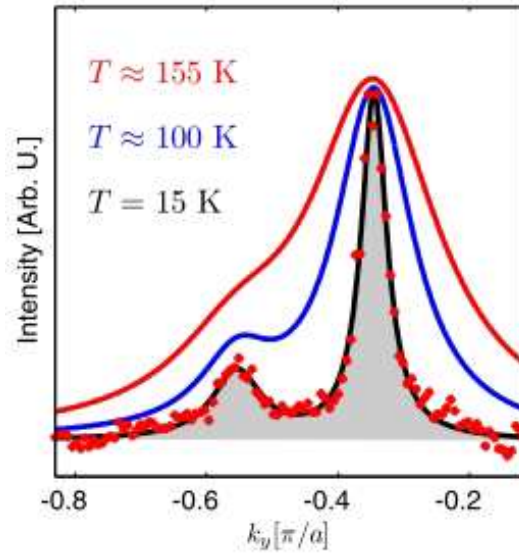


Figure B1. The measured red points sample the MDC at $\omega = E_F$ and $T = 15$ K for the cut (b) while the black line is a double Lorentzian fit with a linear background. The blue and red curves are the extrapolated MDC at $T = 100$ K and $T = 155$ K, respectively, assuming a double Lorentzian fit with a linear background whereby the maximum is taken to be temperature independent while the linewidth increases according to Eq. (1).

- [6] Yelland, E. A. *et al.* Quantum Oscillations in the Underdoped Cuprate $\text{YBa}_2\text{Cu}_4\text{O}_8$. *Phys. Rev. Lett.* **100**, 047003 (2008).
- [7] Bangura, A. F. *et al.* Small Fermi Surface Pockets in Underdoped High Temperature Superconductors: Observation of Shubnikov-de Haas Oscillations in $\text{YBa}_2\text{Cu}_4\text{O}_8$. *Phys. Rev. Lett.* **100**, 047004 (2008).
- [8] Jaudet, C *et al.* de Haas-van Alphen oscillations in the underdoped cuprate $\text{YBa}_2\text{Cu}_3\text{O}_{6.5}$. *arXiv:0711.3559* (2007).
- [9] Norman, M. R., Pines, D and Kallin, C. The pseudogap: friend of foe of the high T_c ? *Adv. Phys.* **54**, 715-733 (2005)
- [10] Lee, P. A. From high temperature superconductivity to quantum spin liquid: progress in strong correlation physics. *Rep. Prog. Phys.* **71**, 012501 (2008)
- [11] Steven A. Kivelson *et al.* How to detect fluctuating stripes in high temperature superconductors *Rev. Mod. Phys.* **75**, 1201 (2003)
- [12] Christensen, N. B. *et al.* Nature of the Magnetic Order in the Charge-Ordered Cuprate $\text{La}_{1.48}\text{Nd}_{0.4}\text{Sr}_{0.12}\text{CuO}_4$. *Phys. Rev. Lett.* **98**, 197003 (2007).
- [13] Chang, J. *et al.* Tuning competing orders in $\text{La}_{2-x}\text{Sr}_x\text{CuO}_4$ cuprate superconductors by the application of an external magnetic field. *arXiv:0712.2181* (2007).
- [14] Tanaka, K. *et al.* Distinct Fermi-Momentum-Dependent Energy Gaps in Deeply Underdoped Bi2212 . *Science* **314**, 1910-1913 (2006).
- [15] Valla, T. *et al.* The Ground State of the Pseudogap in Cuprate Superconductors. *Science* **314**, 1914-1916 (2006).
- [16] Zhou, X. J. *et al.* High-temperature superconductors Universal nodal Fermi velocity. *Nature* **423**, 398-398 (2003).
- [17] Tranquada, J. M. *et al.* Evidence for stripe correlations of spins and holes in copper oxide superconductors. *Nature* **375**, 561-563 (1995).
- [18] Tranquada, J. M. *et al.* Neutron-scattering study of stripe-phase order of holes and spins in

- La_{1.48}Nd_{0.4}Sr_{0.12}CuO₄. Phys. Rev. B **54**, 7489 (1996).
- [19] Ichikawa, N. *et al.* Evidence for stripe correlations of spins and holes in copper oxide superconductors. Phys. Rev. Lett. **85**, 1738 (2000).
- [20] P. Aebi *et al.*, Complete Fermi-surface mapping of Bi₂Sr₂CaCu₂O_{8+x} (001) - coexistence of short-range antiferromagnetic correlations and metallicity in the same phase. Phys. Rev. Lett. **72**, 2757 (1994)
- [21] K. Nakayama *et al.* Origin of shadow bands in single-layered Bi₂Sr₂CuO_{6+δ} studied by high-resolution angle-resolved photoemission spectroscopy. Physica C **460-462**, 931-933 (2007)
- [22] A. Mans *et al.* Experimental proof of a structural origin for the shadow Fermi surface of Bi₂Sr₂CaCu₂O_{8+δ}. Phys. Rev. Lett. **96**, 107007 (2006)
- [23] Warran E. Pickett Electronic structure of the high-temperature oxide superconductors. Rev. Mod. Phys. **61**, 443 (1989)
- [24] The structural transitions from high-temperature tetragonal (HTT) to low-temperature orthorhombic (LTO) structure was measured by neutron scattering for $x = 0.105$, $x = 0.12$ and $x = 0.145$. See: Chang, J. *et al.* Tuning competing orders in La_{2-x}Sr_xCuO₄ cuprate superconductors by the application of an external magnetic field. arXiv:0712.2181 (2007).
- [25] K. Nakayama *et al.* Shadow bands in single-layered Bi₂Sr₂CuO_{6+δ} studied by angle-resolved photoemission spectroscopy. Phys. Rev. B **74**, 054505 (2006)
- [26] X.J. Zhou *et al.* Angle-Resolved Photoemission Spectroscopy on Electronic Structure and Electron-Phonon Coupling in Cuprate Superconductors. Handbook of High-Temperature Superconductivity: Theory and Experiment, edited by J. R. Schrieffer, (Springer, 2007), Page 87-144.
- [27] J.D. Axe and M.K. Crawford Structural instabilities in lanthanum cuprate superconductors. Journal of Low Temperature Physics **95**, 271 (1994)
- [28] M. R. Norman *et al.* Private communication.
- [29] Since the out-of-plane resistivity ρ_c is three orders of magnitude larger than the in-plane resistivity ρ_{ab} in this compound [18] the Fermi surface must be predominantly two-dimensional. The herein applied fermiology model neglects electronic interactions beyond the existence of an energy gap and assumes translation invariance (no impurities).
- [30] Harrison, N. *et al.* Cuprate Fermi Orbits and Fermi Arcs: The Effect of Short-Range Antiferromagnetic Order. Phys. Rev. Lett. **99**, 206406 (2007).
- [31] Notice that although $\gamma \approx \Delta(\pi, 0) \approx 30$ meV it is not clear how they are related. An upper bound on the dimensionless ratio $\gamma a/v_F \ll 1$ follows from the elongated shape of the ellipsoid enclosed by the primary and secondary Fermi arcs, *i.e.*, while the choice of $\gamma = 60$ meV still fits the primary and secondary Fermi arcs, the choice $\gamma = 80$ meV does not. A lower bound on $\gamma a/v_F \ll 1$ follows from the measured ratio of the order 20% between the ARPES intensities along the secondary and primary Fermi arcs. The predicted ratio of ARPES intensities along the secondary and primary Fermi arcs is of the order 0.3% (1%) for $\gamma = 30$ meV ($\gamma = 60$ meV). A pure d -density wave gap $\gamma_{\mathbf{k}} \propto \cos k_x a - \cos k_y a$ is not compatible with the nonvanishing intensity of the secondary Fermi arc close to the diagonal direction.
- [32] Nakamura, Y. & Uchida, S. Anisotropic transport properties of single-crystal La_{2-x-y}Nd_ySr_xCuO₄: Effect of the structural phase transition. Phys. Rev. B **46**, 5841-5844 (1992)
- [33] Noda, T. *et al.* Evidence for One-Dimensional Charge Transport in La_{2-x-y}Nd_ySr_xCuO₄. Science, **286**, 265-268 (1999).
- [34] Adachi, T. *et al.* Crystal growth, transport properties, and crystal structure of the single-crystal La_{2-x}Ba_xCuO₄ ($x = 0.11$). Phys. Rev. B **64**, 144524 (2001).
- [35] D. LeBoeuf, *et al.* Electron pockets in the Fermi surface of hole-doped high-Tc superconductors. Nature, **450**, 533-536 (2007).
- [36] Luttinger, J. M. Fermi Surface and Some Simple Equilibrium Properties of a System of Interacting Fermions. Phys. Rev. **119**, 1153 (1960).

- [37] Notice that A_{ep} compares well with the volume of the electron pocket $A_{ep} = 5.1 \text{ nm}^{-2}$ observed by quantum oscillations in YBCO [5].
- [38] H. Matsui, *et al.* Angle-Resolved Photoemission Spectroscopy of the Antiferromagnetic Superconductor $\text{Nd}_{1.87}\text{Ce}_{0.13}\text{CuO}_4$: Anisotropic Spin-Correlation Gap, Pseudogap, and the Induced Quasiparticle Mass Enhancement. *Phys. Rev. Lett.* **94**, 047005 (2005).
- [39] S. R. Park, *et al.* Electronic structure of electron-doped $\text{Sm}_{1.86}\text{Ce}_{0.14}\text{CuO}_4$: Strong pseudogap effect, nodeless gap, and signatures of short-range order. *Phys. Rev. B* **75**, 060501(R) (2007).
- [40] Kaul, R. K. *et al.* Algebraic charge liquids. *Nature Phys.* **4**, 28-31 (2007).
- [41] Yang, Kai-Yu, *et al.*, Phenomenological theory of the pseudogap state. *Phys. Rev. B* **73**, 174501 (2006). Chen, W.-Q., *et al.*, Quantum oscillations in magnetic-field-induced antiferromagnetic phase of underdoped cuprates: Application to ortho-II $\text{YBa}_2\text{Cu}_3\text{O}_{6.5}$. *EPL*, **82** (2008) 17004.
- [42] Senthil, T. Critical Fermi surfaces and non-fermi liquid metals. *arXiv:0803.4009* (2008).
- [43] Chubukov, A. V. & Morr, D. K. Electronic structure of underdoped cuprates. *Physics Reports* **288**, 355-387 (1997).
- [44] Millis, A. J. & Norman, M. R., Antiphase stripe order as the origin of electron pockets observed in 1/8-hole-doped cuprates. *Phys. Rev. B* **76**, R220503 (2007).
- [45] Chakravarty, S. & Kee H.-Y. Fermi pockets and quantum oscillations of the Hall coefficient in high temperature superconductors. *Proc. Natl. Acad. Sci. USA* **105**, 8835 (2008)
- [46] Mats Granath, Fermi momentum resolved charge order for spin-disordered stripes. *Phys. Rev. B* **77**, 165128 (2008)